

Network Dependence Testing via Diffusion Maps and Distance-Based Correlations

Youjin Lee¹, Cencheng Shen², and Joshua T. Vogelstein^{2,3,4}

¹Department of Biostatistics, Johns Hopkins University

²Center for Imaging Science, Johns Hopkins University

³Department of Biomedical Engineering and Institute for Computational Medicine, Johns Hopkins University

⁴Institute for Computational Medicine, Johns Hopkins University

Abstract

Deciphering the associations between network structure and nodal attributes is one of the core problems in network science. Because the network is often structured and high-dimensional, there are only a few model-based statistical methods available, and the theoretical framework is lacking. In this paper we propose a new approach that tests network dependence via diffusion maps and distance-based correlations. Under exchangeable random graph, the diffusion maps provide a set of exchangeable coordinates, whose latent variables can be interpreted as a generalization of graph spectral embeddings. Upon computing distance-based correlations on the family of diffusion maps, the resulting smoothed maximum statistic is consistent under regularity conditions, optimizes the embedding choice for dependence testing, and enjoys improved power testing than any single embedding. We illustrate the advantages of the proposed test in a wide array of network dependencies throughout simulations and experiments.

Keywords: Adjacency spectral embedding, Diffusion distance, Multiscale generalized correlation (MGC), Normalized graph Laplacian

1 Introduction

The increasing availability and influence of network data have motivated numerous recent advances in statistics and applications in physics, computer science, biology, social science, etc., which poses many new and exciting challenges to data scientists and statisticians due to the distinct structure of network data. A graph, or equivalently a network, is formally defined as an ordered pair $\mathbf{G} = (V, E)$, where V represents the set of nodes (or vertices) and E is the set of edges. The edge connectivity in graph can be conveniently represented by the adjacency matrix $A_n = \{A_n(i, j) : i, j = 1, \dots, n = |V|\}$, with $A_n(i, j)$ being the edge weight between node i and node j , e.g., for an unweighted and undirected network, $A_n(i, j) = A_n(j, i) = 1$ if and only if node i and node j are connected by an edge, and zero otherwise.

This paper focuses on one fundamental and common statistical question – testing independence between the network connectivity and the nodal attributes; that is, given an $n \times n$ adjacency matrix $A_n = \{A_n(i, j)\}$ and the corresponding attributes $X_n = \{x_i \in \mathbb{R}^p : i = 1, \dots, n\}$ associated with each node (or vertex), we would like to test whether the edge connectivity $A_n(i, \cdot)$ has any statistical dependency with the nodal attributes x_i . The standard statistical hypothesis testing is as follows: assume that for each i , $A_n(i, \cdot)$ distributes identically as $F_{\mathbf{a}}$ and x_i distributes identically as $F_{\mathbf{x}}$, the null and alternative hypothesis for network dependence testing is:

$$H_0 : F_{\mathbf{ax}} = F_{\mathbf{a}}F_{\mathbf{x}} \tag{1}$$

$$H_A : F_{\mathbf{ax}} \neq F_{\mathbf{a}}F_{\mathbf{x}},$$

where $F_{\mathbf{ax}}$ denotes the joint distribution. Some real examples are: each person on Facebook

has a number of distinct attributes (e.g., occupations, sex, personal behaviors), and also has connections with other persons and entities via the social network. In neuro-science, each brain region has its own distinct functionality, and is also linked with other regions in the brain map. Therefore, determining the potential associations between edge connectivity and nodal attributes is often a crucial step in exploring the network data.

A notable obstacle in network inference is that the adjacency matrix A_n is structured, e.g., A_n is a symmetric binary matrix under undirected graph, which prevents many well-established methods from being directly used. More specifically, unlike in the traditional data analysis where one can comfortably assume independently and identically distributed (*iid*) of each observation, $A_n(i, \cdot)$ and $A_n(j, \cdot)$ is often dependent based on the actual graph or network model. One approach to tackle the issue is to assume certain model on the graph structure, then solve the inference question based on the model assumption (Wasserman and Pattison, 1996; Fosdick and Hoff, 2015; Howard et al., 2016). For example, the network dependence test proposed by Fosdick and Hoff (Fosdick and Hoff, 2015) assumes that the adjacency matrix is generated from a multivariate normal distribution of the latent factors, estimates the latent factor associated with each node from A_n , followed by applying the standard likelihood ratio test on the normal distribution. Another major approach is spectral embedding, which first embeds the $n \times n$ adjacency matrix into an $n \times q$ projection matrix U by eigen-decomposition, then carries out the later inference task on U (Rohe et al., 2011; Sussman et al., 2012; Tang et al., 2017b,a). However, model-based approaches are often limited by and do not perform well beyond the model assumptions, while the main issue of spectral embedding is that a slight mis-specification of the dimension choice q may significantly degrade the later inference. Indeed, as a ground truth is unlikely in real networks (Peel et al., 2017), one often desires a method that is robust against network model and parameter selection (Chen et al., 2016).

To tackle the challenges, in this paper we propose a new methodology to test network dependency via diffusion maps and distance-based correlations, which is easy to implement, overcomes the limitation of existing methods, has theoretical guarantee, and enjoys superior testing performance. In Section 2, we introduce the diffusion maps to embed the adjacency matrix, and review distance correlation and multiscale generalized correlation (MGC) for testing independence. In Section 3, we formally propose the algorithm named diffusion MGC or DMGC, investigate the theoretical properties of the diffusion map that lead to its testing consistency under permutation test and regularity conditions, which is then connected to existing graph embedding framework under common network models. Section 4 exhibits the numerical successes of the proposed method versus other benchmarks against a number of simulated and real dependency structures. The Appendix contains the proofs, the simulation function details, and additional experiments. The R codes and accompanying data are publicly available online at <http://neurodata.io/tools/mgc>.

2 Preliminaries

2.1 Diffusion Maps

The diffusion map is introduced as a feature extraction algorithm by Coifman and Lafon (Coifman et al., 2005; Coifman and Lafon, 2006; Lafon and Lee, 2006), which computes a family of embeddings in the Euclidean space by eigen-decomposition on a diffusion operator of the given data. Here we introduce one version that tailors to the adjacency matrix.

To derive the diffusion maps for sample observations of size n , the first step is to choose an $n \times n$ kernel matrix K_n that represents the similarity within the sam-

ple data. The adjacency matrix A_n is a natural similarity matrix, thus we take $K_n = (A_n + A_n^T)/2$. Next the kernel matrix is normalized into the Laplacian matrix by $L_n(i, j) = K_n(i, j) / \sqrt{\sum_{j=1}^n K_n(i, j) \sum_{i=1}^n K_n(i, j)}$ when the denominator is positive, and $L_n(i, j) = 0$ otherwise.

Denote q as the embedding dimension and t as the Markov iteration time step, the diffusion map $U_n^t = \{u_i^t : i = 1, \dots, n\}$ is then computed by eigen-decomposition, namely

$$u_i^t = \left(\lambda_1^t \phi_{i1} \quad \lambda_2^t \phi_{i2} \quad \dots \quad \lambda_q^t \phi_{iq} \right) \in \mathbb{R}^q; \quad i = 1, \dots, n, \quad (2)$$

where $\{\lambda_j : j = 1, 2, \dots, q\}$ and $\{\phi_j \in \mathbb{R}^n : (\phi_{1j}, \phi_{2j}, \dots, \phi_{nj}), j = 1, 2, \dots, q\}$ denote the q largest eigenvalues and corresponding eigenvectors of L_n , and λ_j^t denotes the t^{th} power of the j^{th} eigenvalue. The diffusion distance between the i^{th} observation and the j^{th} observation is defined as the weighted L^2 distance of the two points in the observation space, which equals the Euclidean distance in the diffusion coordinate (Coifman and Lafon, 2006):

$$C^t(i, j) = \|u_i^t - u_j^t\|; \quad i, j = 1, 2, \dots, n,$$

where $\|\cdot\|$ is the Euclidean distance.

When $t = 0$, the diffusion map is exactly the same as a normalized graph Laplacian embedding in Rohe et al. (2011) up-to a linear transformation; when $t > 0$, the diffusion maps are weighted graph Laplacian by powered eigenvalues (Lafon and Lee, 2006); and the diffusion map at $t = 1$ equals the adjacency spectral embedding (ASE) up-to the degree constant (Sussman et al., 2014). Therefore, the diffusion maps can be viewed as a collection of embeddings controlled by a single parameter $t \in [0, \infty]$. The embedding dimension choice q can be selected via the profile likelihood method in Zhu and Ghodsi (2006), which is a

standard algorithm in dimension reduction literature. To select the optimal t , we will utilize a smoothing technique unique to testing independence in Section 3.1.

2.2 Distance-Based Correlations

The problem of testing general dependencies between two random variables has seen notable progress in recent years. The Pearson’s correlation (Pearson, 1895) is the most classical approach, which determines the existence of linear relationship via a correlation coefficient in the range of $[-1, 1]$, with 0 indicating no linear association and ± 1 indicating perfect linear association. To better capture the dependencies not limited to linear relationship, a variety of distance-based correlation measures have been suggested, including the Mantel coefficient (Mantel, 1967), distance correlation (dCorr) and energy statistic (Székely et al., 2007; Székely and Rizzo, 2013a; Rizzo and Székely, 2016), kernel-based independence test (Gretton and Györfi, 2010), Heller-Heller-Gorfine (HHG) test (Heller et al., 2013, 2016), and multiscale generalized correlation (MGC) (Shen et al., 2017a,b), among others. In particular, distance correlation is the first correlation measure that is consistent against all possible dependencies with finite first moment. The multiscale generalized correlation (MGC) statistic inherits the same consistency of distance correlation with remarkably better finite-sample testing powers under high-dimensional and nonlinear dependencies, via defining a family of local correlations and efficiently searching for the optimal local scale in testing. Here we briefly introduce dCorr and MGC.

Given a pair of sample data $(U_n, X_n) = \{(u_i, x_i) : i = 1, 2, \dots, n\}$ that are *iid* as $F_{\mathbf{u}\mathbf{x}} \in \mathbb{R}^q \times \mathbb{R}^p$. Denote the pairwise distances within $\{u_i\}_{i=1}^n$ and $\{x_i\}_{i=1}^n$ as $C(i, j) = \|u_i - u_j\|$ and $D(i, j) = \|x_i - x_j\|$ for $i, j = 1, 2, \dots, n$ respectively. The distance covariance between

the sample data is defined as

$$\mathbf{dCov}(U_n, X_n) = \frac{1}{n^2} \sum_{i,j=1}^n \tilde{C}(i, j) \tilde{D}(i, j), \quad (3)$$

where \tilde{C} and \tilde{D} doubly-center C and D by its column mean and row mean respectively, i.e., $\tilde{C} = HCH$, where $H = I_{n \times n} - J_{n \times n}/n$ (the double centering operation matrix), $I_{n \times n}$ is the $n \times n$ identity matrix (ones on the diagonal, zeros elsewhere), and $J_{n \times n}$ is the $n \times n$ matrix of all ones. The distance correlation (\mathbf{dCorr}) follows by normalizing distance covariance by distance variances and thus lies in the range of $[0, 1]$. In Székely et al. (2007), \mathbf{dCorr} has been shown to be asymptotically 0 if and only if independence, i.e., $F_{\mathbf{u}\mathbf{x}} = F_{\mathbf{u}}F_{\mathbf{x}}$, resulting in a consistent statistic for independence testing; an unbiased sample version of distance correlation is later proposed to eliminate the sample bias in \mathbf{dCorr} (Székely and Rizzo, 2013b, 2014), which is the default for \mathbf{dCorr} implementation in this paper.

The **MGC** statistic is an optimal local version of distance correlation, aiming for improved finite-sample testing power. Along the same line as \mathbf{dCorr} , it first derives all local distance covariances \mathbf{dCov}^{kl} as

$$\mathbf{dCov}^{kl}(U_n, X_n) = \frac{1}{n^2} \sum_{i,j=1}^n \tilde{C}^k(i, j) \tilde{D}^l(i, j); \quad k, l = 1, \dots, n,$$

where $\tilde{C}^k(i, j) = \tilde{C}(i, j)\mathbf{I}(R_{ij}^C \leq k)$, $\mathbf{I}(\cdot)$ is the indicator function, and R_{ij}^C is a rank function of u_i relative to u_j , i.e., $R_{ij}^C = k$ if u_i is the k^{th} nearest neighbor of u_j , and define equivalently $\tilde{D}^l(i, j) = \tilde{D}(i, j)\mathbf{I}(R_{ij}^D \leq l)$ for $\{x_i\}$. Then the local distance correlations $\{(\mathbf{dCorr}^{kl})\}$ are the normalizations of the local distance covariances into $[-1, 1]$. Among all possible neighborhood choices, the **MGC** statistic equals the maximum local correlation within the

largest connected component of significant local correlations, i.e.,

$$\text{MGC}(U_n, X_n) = \text{dCorr}^{(kl)^*}(U_n, X_n), \text{ where } (kl)^* = \arg \max_{(kl)} S(\text{dCorr}^{kl})$$

for a smoothing operation $S(\cdot)$ that filters out all in-significant local correlations.

MGC has been shown to have power almost equal or better than dCorr throughout various types of general dependencies. Despite searching over all possible neighborhoods for the optimal local correlation, it is also computationally efficient with a similar running time complexity as dCorr and HHG . The details on the population statistic, sample version on unbiased dCorr , and running time analysis are available in [Shen et al. \(2017a\)](#).

3 Main Results

The main method is named **DMGC** (diffusion MGC), which synthesizes diffusion map embedding, distance-based measure by **MGC**, and optimal correlation smoothing. The testing method is presented first, followed by exchange-ability of diffusion maps and testing consistency under regularity conditions in Section 3.2, which are further elaborated in Section 3.3 under the random dot product graph model. All proofs are supplied in Appendix A.

3.1 Testing procedure of Diffusion MGC

Input: The adjacency matrix $A_n \in \mathbb{R}^{n \times n}$ representing the edge connectivities, and the nodal attributes $X_n = \{x_i \in \mathbb{R}^p : i = 1, 2, \dots, n\}$. The input graph can be of any structure, e.g., directed or undirected, weighted or unweighted, connected or disconnected, has self-loop or not.

Step 1 (Diffusion Map Embedding): Compute a collection of diffusion embeddings

$\{U_n^t = \{u_i^t, i = 1, \dots, n\}, t = 0, 1, 2, \dots, 10\}$: Transform the adjacency matrix into a symmetric kernel matrix as $K_n(i, j) = (A_n(i, j) + A_n(j, i))/2$, compute the Laplacian matrix L_n , select the dimension q as the second elbow of the absolute eigenvalues of L_n , and compute the embeddings $\{U_n^t\}$.

Step 2 (MGC Computation): For each t , calculate the MGC statistic $\text{MGC}(U_n^t, X_n)$.

Step 3 (DMGC by Smoothing): Takes the DMGC statistic $\text{MGC}^*(\{U_n^t\}, X_n)$ as the smoothed maximum among $\{\text{MGC}(U_n^t, X_n), t = 0, 1, 2, \dots, 10\}$: if there exists a t^* such that $[\text{MGC}(U_n^{t^*-1}, X_n), \text{MGC}(U_n^{t^*}, X_n), \text{MGC}(U_n^{t^*+1}, X_n)]$ are the three largest statistics among all, take $\text{MGC}^*(\{U_n^t\}, X_n) := \text{MGC}(U_n^{t^*}, X_n)$. Otherwise, $\text{MGC}^*(\{U_n^t\}, X_n) = \text{MGC}(U_n^{t=3}, X_n)$ (note that when checking $t = 0$ and $t = 10$, we only check the one-sided adjacent time step instead of two-sided, so t^* can be 0 or 10).

Step 4 (Permutation Test): Compute the p-value of the DMGC statistic via the permutation test. Given any permutation σ of size n , we randomly permute the sample indices of the nodal attributes as $X_n^\sigma = \{x_{\sigma(i)}\}$ (but keep the ordering of diffusion maps), repeat step 2 and 3 to compute the permuted DMGC statistic $\text{MGC}^*(\{U_n^t\}, X_n^\sigma)$. Generating r random permutations, the p-value equals the proportion of times that the permuted DMGC is no smaller than the original DMGC.

Output: The DMGC statistic $\text{MGC}^*(\{U_n^t\}, X_n)$, the optimal time step t^* , and the p-value by permutation test. The independence hypothesis is rejected if the p-value is less than a given critical level α .

The motivation of the smoothed maximum in Step 3 is the following: suppose that edge connectivity is truly dependent with the attributes, and there exists an optimal t for detecting the relationship, then the test statistic at adjacent time steps should also exhibit

strong signal, because the level of connectivity considering all paths of length t between each pair is most similar to those of length $t - 1$ or $t + 1$. Under independence, a large test statistic at certain t can occur by chance and cause a direct maximum to have a low testing power, while the smoothed maximum effectively filters out any noisy and isolated large test statistic. In practice, it suffices to consider $t \in [0, 1, \dots, 10]$ or even smaller upper bound like 3 or 5. When smoothed maximum does not exist, we set $t = 3$ as the default choice.

The permutation test is a common nonparametric procedure used for real data testing in almost all dependency measures (Székely et al., 2007; Heller et al., 2013; Gretton and Györfi, 2010; Shen et al., 2017a). Because the null distribution of any correlation measure depends on the marginal distribution and is difficult to obtain, the permutation test breaks the dependence of the given data while keeping the marginal distributions, and is thus able to empirically approximate the null distribution.

A flowchart of the above procedure is provided in Figure 1. Note that the algorithm is flexible in the choice of correlation measures: by following the exact same steps except replacing MGC by dCorr / HHG / other correlation measure in Step 2, one can compute the diffusion dCorr or diffusion HHG statistic.

3.2 Theoretical Properties Under Exchangeable Graph

To derive the theoretical properties of our methodology, the following distributional conditions on the graph \mathbf{G} and the nodal attributes X_n are required:

(C1) Graph \mathbf{G} is an induced subgraph of an infinitely exchangeable graph, i.e., the adja-

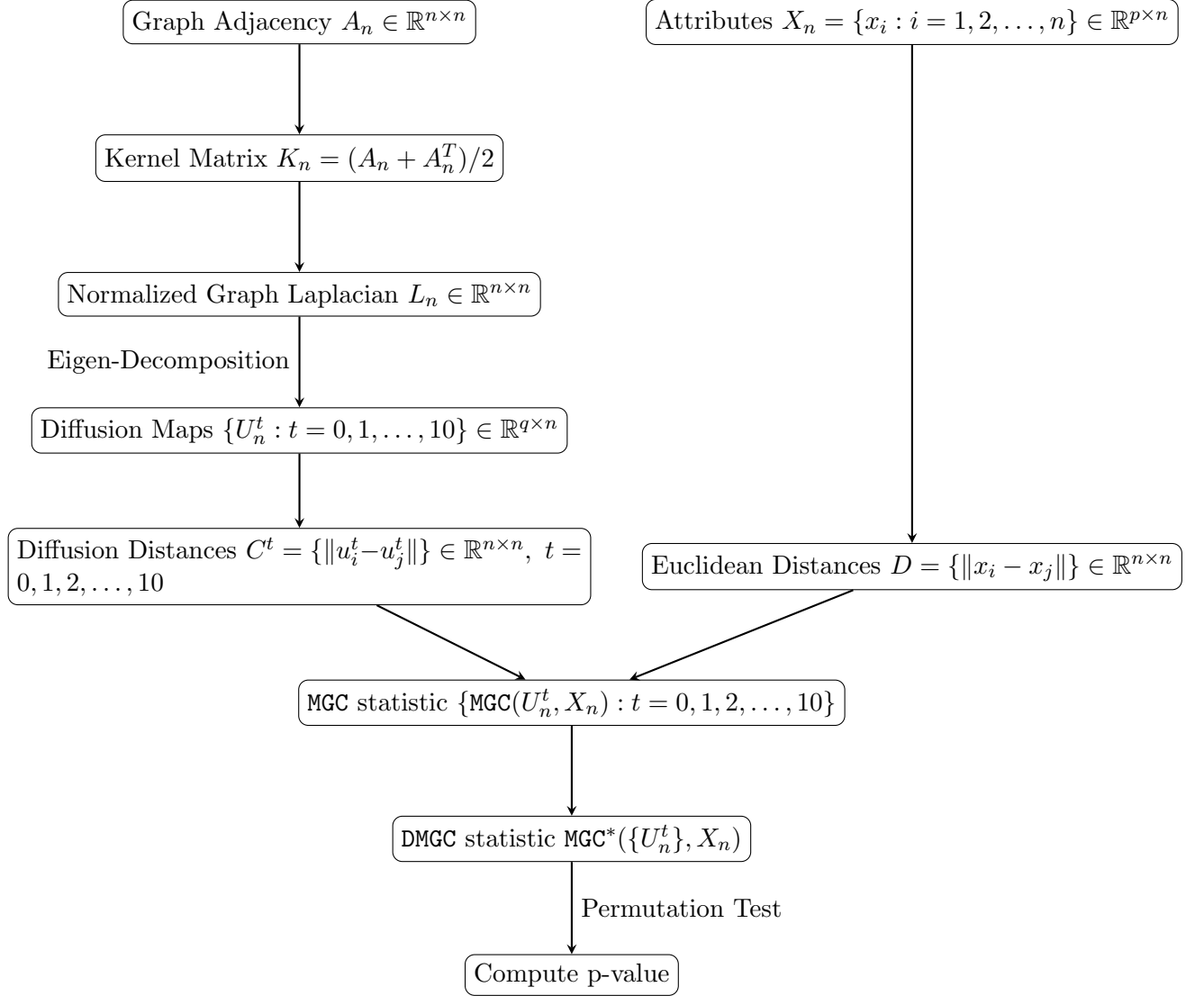


Figure 1: Flowchart for Network Dependence Testing via Diffusion Maps and MGC (DMGC).

gency matrix A_n is generated by a $n \times n$ random matrix \mathbf{A}_n such that

$$\mathbf{A}_n(i, j) \stackrel{d}{=} \mathbf{A}_n(\sigma(i), \sigma(j))$$

for any $i, j = 1, 2, \dots, n$ and any permutation σ of size $n \in \mathbb{N}$. The notation $\stackrel{d}{=}$ stands for equality in distribution.

(C2) Assume each nodal attribute x_i is independent and identically distributed as $F_{\mathbf{x}}$ with finite first moment.

(C3) The random matrix \mathbf{A}_n is constrained to a domain Ω , and there exists some t such that the diffusion map embedding from $A_n \in \Omega$ to U_n^t is injective.

Condition (C1) is straightforward to verify and satisfied by many popular statistical networks models. Based on condition (C1), the diffusion map U_n^t at each t can furnish exchangeable / asymptotic conditional *iid* embedding for the set of nodes $V(\mathbf{G})$.

Theorem 1. *Assume \mathbf{G} satisfies (C1). Then at each fixed t , the diffusion map $\{u_i^t, i = 1, 2, \dots, n\}$ for each node are exchangeable. As a result, there exists a latent variable \mathbf{u}^t such that u_i^t are iid conditional on \mathbf{u}^t for $i = 1, 2, \dots, n$ as $n \rightarrow \infty$.*

The exchangeable / asymptotic conditional *iid* property of the diffusion map leads to the consistency of DMGC for testing independence between \mathbf{u}^t and \mathbf{x} of finite first moment. In that sense, condition (C2) is merely a regularity condition for \mathbf{x} , while \mathbf{u}^t always satisfies the finite-moment assumption (shown in appendix proof of Theorem 2). The next theorem is a direct extension of the consistency proofs from Székely et al. (2007) and Shen et al. (2017a) to exchangeable random variables.

Theorem 2. *Assume the graph \mathbf{G} and the attributes X_n satisfy condition (C1) and (C2). Then as $n \rightarrow \infty$, the MGC statistic between the diffusion map U_n^t at any fixed t and the nodal attributes X_n satisfies:*

$$MGC(U_n^t, X_n) \rightarrow c \geq 0,$$

with equality holds if and only if \mathbf{u}^t is independent of \mathbf{x} .

The consistency of DMGC follows in the next theorem. Moreover, DMGC is not only consistent between diffusion map and nodal attributes, but also consistent between edge connectivity and nodal attributes if condition (C3) is satisfied.

Theorem 3. *Under the same assumption in Theorem 2, it holds that*

$$\text{MGC}^*(\{U_n^t\}, X_n) \rightarrow c \geq 0,$$

with equality holds if and only if \mathbf{u}^t is independent of \mathbf{x} for all $t \in [0, 10]$. Therefore, DMGC is a valid and consistent statistic for testing independence between the diffusion maps $\{U_n^t\}$ and nodal attributes X_n .

If condition (C3) holds, then $\text{MGC}^*(\{U_n^t\}, X_n)$ is also valid and consistent for testing independence between the adjacency matrix A_n and nodal attributes X_n , i.e., it converges to 0 if and only if \mathbf{a} and \mathbf{x} are independent.

Interpreted in another view, DMGC is always valid to use, but may not always detect the dependency between the adjacency matrix A_n and nodal attributes X_n if the dependency signal is lost during the embedding. Therefore, condition (C3) on injective transformation is a sufficient condition to preserve the dependency signal for diffusion map.

Corollary 1. Theorem 3 still holds, when any of the following changes are applied to the testing procedure described in Section 3.1:

- (1) The nodal attributes in the input are replaced by a second graph of the same node set, followed by the same diffusion map process;
- (2) The MGC statistic in step 2 is replaced by dCorr or HHG;

- (3) When \mathbf{A}_n is restricted to be symmetric, binary, and of finite rank $q < n$, then condition (C3) holds at $t = 1$.

Namely, point (1) shows that the same approach can be applied to a paired graph-test of arbitrary structures, e.g., testing between a weighted directed graph and an unweighted undirected graph, by deriving the diffusion maps for each graph individually. Point (2) suggests that under diffusion maps, consistent distance-based measures such as `dCorr` and `HHG` can also be used instead of `MGC`. To that end, we can compare `DMGC` to diffusion `dCorr` and `HHG` in the simulations. And point (3) offers an example of \mathbf{A}_n where the diffusion map is guaranteed injective within the domain.

3.3 Theoretical Properties Under Random Dot Product Graph

In this section, we consider the random dot product graph model (RDPG), which is widely used in network modeling and ideal for illustration. A RDPG is an exchangeable graph model, for which the latent position under RDPG can be asymptotically recovered by diffusion maps.

A graph generated from RDPG model has an edge probability as a dot product of *iid* node-wise latent position: assuming each node has a latent position $w_i \stackrel{iid}{\sim} F_{\mathbf{w}}$ for $i = 1, 2, \dots, n$, the edge probability $P(\mathbf{A}_n(i, j) = 1 | w_i, w_j)$ is determined by the dot product of the latent positions, i.e.,

$$\mathbf{A}_n(i, j) | w_i, w_j \stackrel{iid}{\sim} \text{Bern}(\langle w_i, w_j \rangle), i, j = 1, 2, \dots, n \text{ and } i < j.$$

under the restriction that all w_i 's are non-negative vectors and the dot product must be normalized within $[0, 1]$.

A RDPG is an exchangeable graph model that satisfies condition (C1). In addition,

RDPG fully specifies all exchangeable graph models that are unweighted and symmetric, whose probability generating matrix $\mathcal{P}_n(i, j) = \langle w_i, w_j \rangle$ is positive semi-definite.

Proposition 1 (Sussman et al. (2014)). An exchangeable random graph has a finite rank q and positive semi-definite link matrix \mathcal{P}_n , if and only if the random graph is distributed according to a random dot product graph with *iid* latent vectors $\{w_i \in \mathbb{R}^q, i = 1, \dots, n\}$.

Indeed, many other popular network modeling are special cases of RDPG, including the stochastic block model, its degree-corrected version, the latent factor model from Fosdick and Hoff (2015), etc.

Proposition 2 (Rohe et al. (2011)). Let L_n be the normalized graph Laplacian for an adjacency matrix A_n generated by an RDPG with latent positions $W_n = [w_1, w_2, \dots, w_n] \in \mathbb{R}^{q \times n}$. Then there exists a fixed diagonal matrix M and an orthonormal rotational matrix $Q \in \mathbb{R}^{q \times q}$ such that $\|U_n^{t=1} - QMW_n\| \rightarrow 0$ almost surely.

Therefore, under RDPG, the latent variable of the diffusion map $\mathbf{u}^{t=1}$ asymptotically equals the latent position \mathbf{w} up to a linear transformation, and DMGC is consistent against testing general dependency between \mathbf{a} and \mathbf{x} .

Corollary 2. Under the finite-dimensional exchangeable graph with positive semi-definite link function, the DMGC statistic is consistent for the hypothesis in Equation 1.

Alternatively, one can utilize the adjacency spectral embedding to establish the equivalence via $\mathbf{u}^{t=1}$. Existing network inference mostly relies on a single embedding choice, whose theoretical properties are often guaranteed but may fall short in practice when the embedding choice deviates from the truth. Our DMGC approach utilizes a collection of $\{\mathbf{u}^t\}$ to identify the strongest dependence signal, thus optimizes over the family of diffusion maps and shall perform better than any single embedding scheme. This procedure also

avoids multiple testing and cross validation, which makes the network testing procedure theoretically sound.

4 Numerical Studies

In this section, we demonstrate the advantages of our approach via simulations and real data experiment. Throughout the numerical studies, we compare **DMGC** to the likelihood ratio test proposed by Fosdick and Hoff (FH) (Fosdick and Hoff, 2015), single embedding tests (using the adjacency spectral embedding **AM** and the latent factors **LF** with distance-based tests like **dCorr** and **HHG**), and two variants of **DMGC** (diffusion **dCorr** and **HHG**). The main approach of **DMGC** is denoted as **MGC** \circ **DM**, and the benchmarks are **FH**, **MGC**/**dCorr**/**HHG** \circ **AM**/**LF**/**DM**.

For each simulation, we generate a sample graph and the corresponding attributes, compute the correlation measure on the respective embedding, carry out the permutation test with $r = 500$ random samples for each method, and reject the null if the resulting p-value is less than $\alpha = 0.05$. The testing power of each method equals the percentage of correct rejection out of $nr = 100$ Monte-Carlo replicates, and a higher power implies a better method against the given dependency structure.

4.1 Stochastic Block Model

The first simulation generates graphs by the stochastic block model (SBM), which is one of the most popular network models which many network methodologies have been built on. The SBM assumes that each of n nodes in \mathbf{G} must belong to one of $K \in \mathbb{N}$ blocks, and determines the edge probability based on the block-membership of the connecting nodes: For $i = 1, \dots, n$, assume that a latent variable of $z_i \stackrel{iid}{\sim} Multinomial(\pi_1, \pi_2, \dots, \pi_K)$ denotes

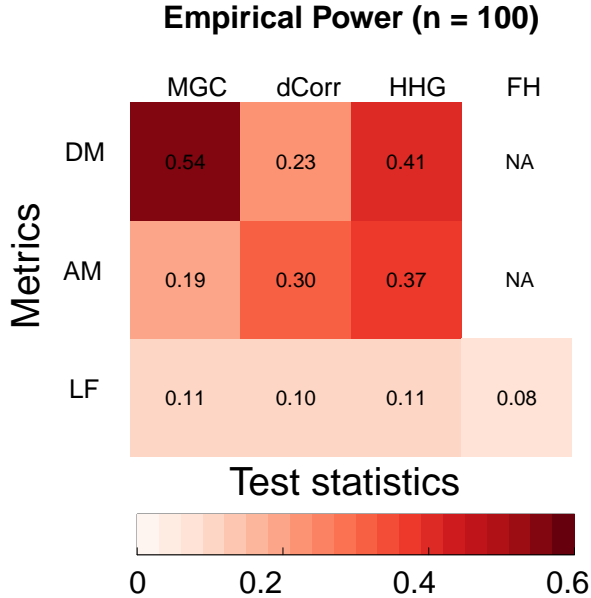


Figure 2: The power heatmap under the three-block SBM (Equation 4) demonstrates that among all possible combinations of test statistics with distance metrics, DMGC (top left entry) provides the best power.

the block-membership of each node, and $p_{kl} \in [0, 1]$ implies the edge probability between any two nodes of class k and l respectively; then the upper triangular entries of A_n are independently and identically distributed conditioned on $Z_n = \{z_i : i = 1, 2, \dots, n\}$:

$$\mathbf{A}_n(i, j) | z_i, z_j \stackrel{iid}{\sim} \text{Bernoulli}\left(\sum_{k,l=1}^K p_{kl} \mathbf{I}(z_i = k, z_j = l)\right); \quad i < j, \quad i, j = 1, 2, \dots, n,$$

where $\mathbf{I}(\cdot)$ is the indicator function.

It is of common interest to detect whether the block structure has anything to do with the edge connectivity; and noisy information on the block structure often better reflects reality and adds difficulty to the testing. Thus we consider testing dependency between the graph having the adjacency matrix A_n and a noisy block-membership X_n , which are

correlated through true block-membership Z_n :

$$\begin{aligned}
 z_i &\stackrel{i.i.d.}{\sim} \text{Multinom}(1/3, 1/3, 1/3), \\
 E(\mathbf{A}_n(i, j)|z_i, z_j) &= 0.5\mathbf{I}(|z_i - z_j| = 0) + 0.2\mathbf{I}(|z_i - z_j| = 1) + 0.4\mathbf{I}(|z_i - z_j| = 2), \quad (4) \\
 x_i|z_i &\sim \text{Multinom}((1 + \mathbf{I}(z_i = 1))/4, (1 + \mathbf{I}(z_i = 2))/4, (1 + \mathbf{I}(z_i = 3))/4),
 \end{aligned}$$

and we set the sample size at $n = 100$. Equation 4 implies that the within-block edge probability is always 0.5; while the between-block edge probability is 0.2 when the block labels differ by 1, and 0.4 when the block labels differ by 2. A visualization of the sample data is shown in Figure 7a. Note that nodal attributes X_n from the above model contaminates the true block-membership by: for each i , $x_i = z_i$ with probability 0.5, and equally likely to take other values in Ω , i.e., the true block-membership are observed half of the time. Notably, although within-block edge probability is the largest, the between-block edge probability is not linearly related to the distance of the block-membership, i.e., the edge probability between a node of block 1 and a node of block 3 is higher than the edge probability between block 1 and block 2.

Therefore, this three-block SBM generates a noisy and nonlinear dependency structure between A_n and X_n . Here DMGC is expected to work better than all the other combinations mainly because MGC captures the nonlinear dependency better than dCorr, HHG, and the standard likelihood ratio test. Indeed, Figure 2 shows that DMGC prevails in the testing powers among all the methods.

In the next few experiments, we compare the number of benchmarks and illustrate the advantage of DMGC in terms of the use of the MGC statistic, network embeddings of diffusion maps, and its robustness against parameters, under a wide range of different dependencies.

4.2 SBM with Linear and Nonlinear Dependencies

To better understand the advantage of our main approach (MGC \circ DM) under different scenarios, here we use the same three-block SBM and its block-membership $\{z_i : i = 1, 2, \dots, n = 100\}$ as in the previous section, except that the edge probability is now controlled by $\theta \in (0, 1)$ as follows:

$$E(\mathbf{A}_n(i, j) | z_i, z_j) = 0.5\mathbf{I}(|z_i - z_j| = 0) + 0.2\mathbf{I}(|z_i - z_j| = 1) + \theta\mathbf{I}(|z_i - z_j| = 2); \quad i < j = 1, \dots, n. \quad (5)$$

The noisy block-membership X_n is generated in the same way as before.

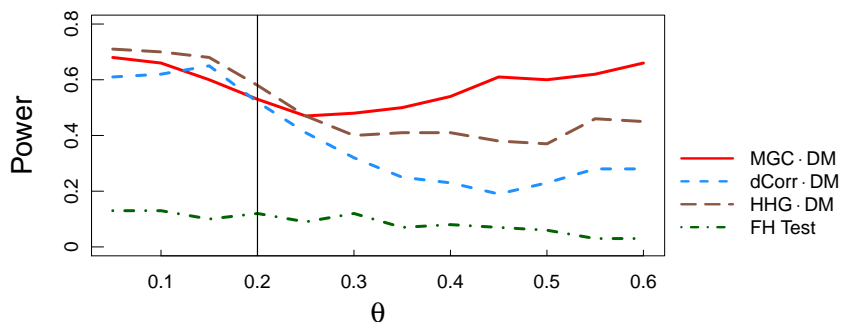


Figure 3: The power curve with respect to increasing θ under three-block SBM (Equation 5). When $\theta \leq 0.2$, the dependency is close to linear dependency between the adjacency matrix and the block structure; when $\theta > 0.2$, the dependency becomes more and more nonlinear as θ gets further away from 0.2. Among all methods utilizing diffusion maps, MGC is evidently the best performing one when $\theta \geq 0.25$, implying that it better captures nonlinear dependencies.

When $\theta = 0.2$, the three-block SBM is the same as a two-block SBM, where within-block edge probability equals 0.5 while the between-block edge probability is always 0.2, i.e., it represents a linear association between the adjacency matrix and the block-membership;

when $\theta < 0.2$, the association is still monotonic; when $\theta > 0.2$ and gets further away, the relationship becomes strongly nonlinear. Figure 3 plots the power against θ for all diffusion maps based methods. All of diffusion **MGC**, diffusion **dCorr**, and diffusion **HHG** perform almost the same at linear dependency (i.e, $\theta \leq 0.2$), with diffusion **MGC** (**DMGC**) being significantly more powerful as the dependency shifts to strong nonlinearity and even increasing as θ increases. This observation demonstrates empirically that **MGC** better captures nonlinear dependencies in network testing for these settings.

4.3 Degree-corrected SBM

In this section we compare different embeddings under the degree-corrected stochastic block model (DC-SBM), which better reflects many real-world sparse networks (Karrer and Newman, 2011). The DC-SBM is an extension of SBM by introducing an additional random variable c_i to control the degree of each node.

We set $n = 200$ with two blocks, select the binary block-membership z_i uniformly in $\Omega = \{0, 1\}$, and generate the edge probability by

$$E(\mathbf{A}_n(i, j) | z_i, z_j, c_i, c_j) = 0.2c_i c_j \cdot \mathbf{I}(|z_i - z_j| = 0) + 0.05c_i c_j \cdot \mathbf{I}(|z_i - z_j| = 1), \quad (6)$$

where $c_i \stackrel{iid}{\sim} Uniform(1 - \tau, 1 + \tau)$ for $i = 1, \dots, n$, and $\tau \in [0, 1]$ is a parameter to control the amount of variability in the edge degree, e.g., as τ increases, the model becomes more complex as the variability of the edge probability becomes larger; when $\tau = 0$, the above model reduces to a two-block SBM without any variability induced by $\{c_i : i = 1, 2, \dots, n\}$.

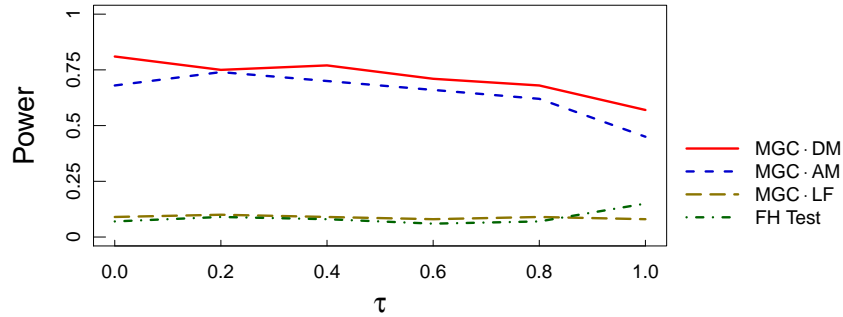


Figure 4: The power curve with respect to increasing τ under DC-SBM (Equation 6). The edge variability increases as τ does, the testing power of diffusion maps is relatively stable against increasing variability; the adjacency spectral embedding is slightly worse, while the latent positions fail to detect the dependency across all levels of τ .

Similar as before, we generate the nodal attributes X_n as a noisy version of the true block-membership via Bernoulli distribution, i.e., for each i , $x_i = z_i$ with probability 0.6, and equals the wrong label with probability 0.4. Under DC-SBM, DMGC also has superior power. In particular, Figure 4 compares different embeddings with MGC, which shows that $\text{MGC} \circ \text{DM}$, i.e. DMGC, has a better testing performance over the other embedding methods throughout τ .

4.4 RDPG Simulations

Here we present a variety of RDPG simulations by generating the latent variables via the 20 relationships in Shen et al. (2017a) with different levels of noise, consisting of various close-to-linear and nonlinear relationships. The details of simulation schemes are in

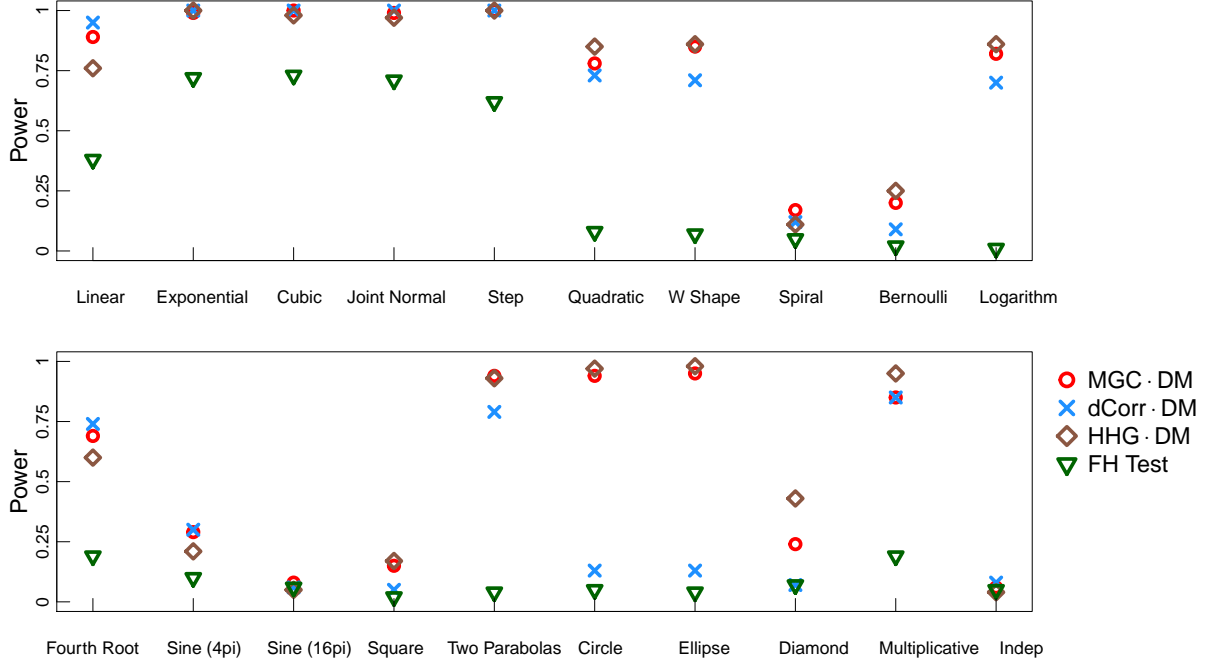


Figure 5: Power comparison for 20 different RDPGs presented in the Appendix B with $n = 50$ nodes per $nr = 100$ independent replicates. It shows that when latent positions W_n and nodal attributes X_n are dependent via a close-to-linear relationship (upper panel), all the distance-based tests achieve similar power while FH test is slightly worse due to its model-based nature. When non-linearity between W_n and X_n becomes evident like circle or ellipse (lower panel), dCorr and FH tests are far behind than MGC and HHG.

Appendix B while a general outline for data generating process is:

$$\begin{aligned} \left(\tilde{w}_i \quad \tilde{x}_i \right) &\stackrel{iid}{\sim} F_{\tilde{\mathbf{w}}, \tilde{\mathbf{x}}} \\ \mathbf{A}_n(i, j) | w_i, w_j &\sim \text{Bern}(\langle w_i, w_j \rangle), \quad i < j = 1, 2, \dots, n, \end{aligned} \quad (7)$$

where $w_i = (\tilde{w}_i - \min(\{\tilde{w}_j : j = 1, 2, \dots, n\})) / (\max(\{\tilde{w}_j : j = 1, 2, \dots, n\}) - \min(\{\tilde{w}_j : j = 1, 2, \dots, n\}))$ for $i = 1, 2, \dots, n$, so that all the latent variable range from 0 to 1. We apply

the same scaling from \tilde{X}_n to X_n for visual consistency.

Thus the latent positions W_n and nodal attributes X_n are correlated via a joint distribution of $F_{\tilde{w}, \tilde{x}}$, which includes linear / quadratic / circle, etc. Figure 5 shows empirical power obtained from $nr = 100$ independent replicates when the number of nodes is $n = 50$. A lack of power in the FH test is evident even though data generative model in Equation 7 agrees with Fosdick and Hoff (2015)'s, mainly due to mis-specification of network factor dimension.

All the distance-based methods work fairly well, with diffusion MGC and diffusion HHG being the best performers. Note that the last scenario is an independent relationship and all tests achieve a power approximately at 0.05, implying that they are all valid tests; there are also a few dependencies of very low power due to the complexity of the relationship (sine, spiral, square, etc.), but their powers all converge to 1 as sample size n increases.

4.5 Parameter Selection and Smoothed Maximum

To support the robustness of DMGC in terms of parameter selection, in this subsection we empirically verify the choice of q and smoothing maximum of t . As a reminder, the dimension choice q is selected by the second elbow of the absolute eigenvalue scree plot by the profile likelihood method from Zhu and Ghodsi (2006), which is a widely-used automatic algorithm for selecting the number of important features whenever eigenvalues or singular values are involved. The choice of t^* is based on a smoothing maximum, i.e., we take the maximum correlation only when consecutive MGC statistics are also large. Neither involves cross validation, and we investigate how well the parameter selection works and how robust our procedure is.

Figure 6 presents the diffusion distances at different t and q for the three-block stochastic block model in Equation 4. Although the resulting embedding is sensitive to both t and q

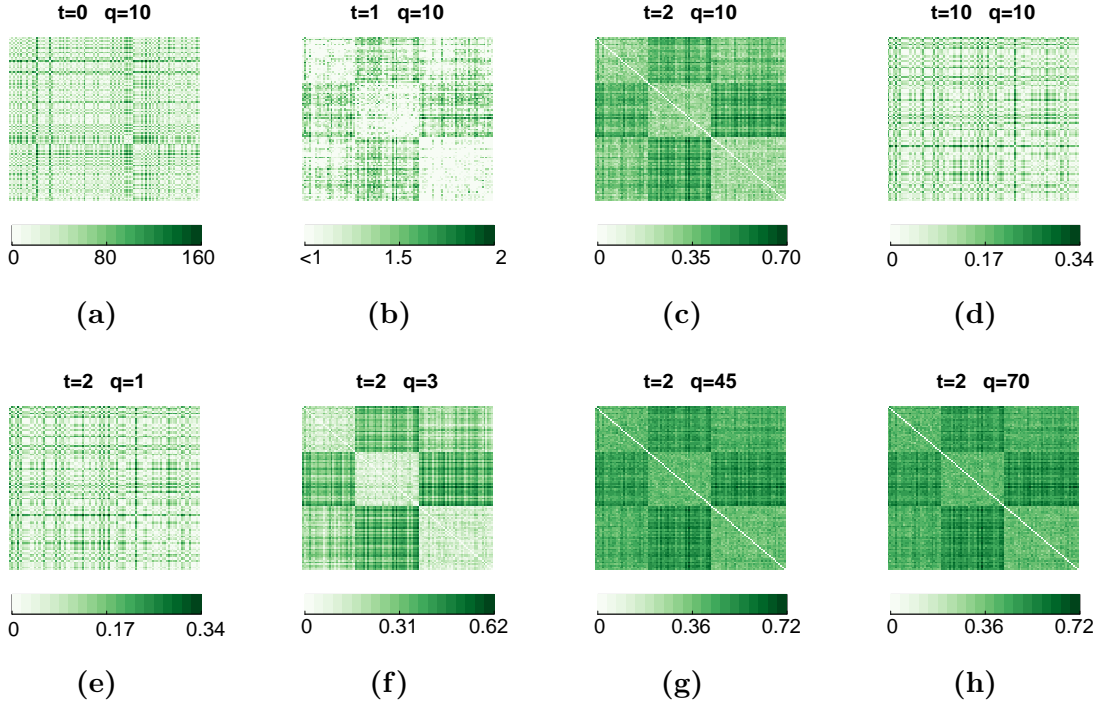


Figure 6: Generate a three-block adjacency matrix A_n by Equation 4 at $n = 100$, and compute the diffusion distances at each combination of (t, q) . A visualization of adjacency matrix is provided in Figure 7a, and it is clear that upon fixing a “good” t , most choices of q still preserve the block structure. Note that the first three elbows of eigenvalues are $(1, 45, 70)$ respectively.

in Figure 6a - 6d, once optimal t^* is fixed it is robust against q , e.g., Figure 6e - 6h show that for a wide range of q the block structure is preserved in the resulting diffusion maps, including the second or third elbow choice.

On the other hand, a fixed embedding choice without optimal t selection is often sensitive to the choice of q . Using the same example, Figure 7 shows the Euclidean distance of the adjacency spectral embedding (ASE) (Sussman et al., 2012) applied to the same adjacency matrix. For ASE, the correct dimensional choice equals the number of blocks, i.e., the distance matrix at $q = 3$ shows a clear block structure (Figure 7b). However, a

slight mis-specification of q can cause the embedding to have a more obscure block structure, and the elbow method often fails to find the correct q for ASE. Note that up to

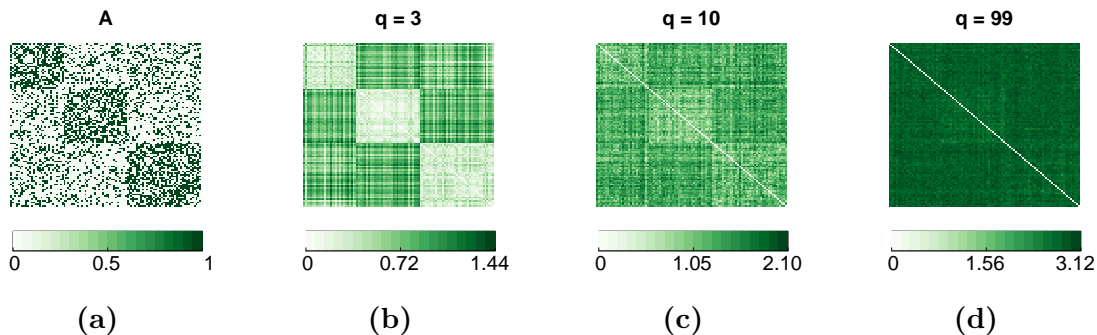


Figure 7: Panel (a) shows the adjacency matrix of three-block adjacency matrix A_n generated by Equation 4. Panel (b)-(d) show the Euclidean distance matrix of ASE at increasing q , using the same adjacency matrix of Panel (a). Only ASE at $q = 3$, namely at the correct dimension, is able to display a clear block structure. Note that the first three elbows are $(1, 45, 70)$, so that it is difficult for ASE to recognize the block structure when the dimension is chosen via the scree plot.

a linear transformation, both normalized Laplacian embedding and ASE equal diffusion map at $t = 1$; consequently, a fixed time t may not couple well with q as illustrated in Figure 6. On the other hand, DMGC successfully mitigates the issue by selecting the optimal t^* that maximizes the signal under the elbow-selected q . Next we compare the optimal t^* by diffusion MGC versus each fixed t . Figure 8 shows the proportion of choosing t as the optimal among $\{0, 1, 2, \dots, 10\}$. Figure 8a illustrates that under the SBM dependency structure in Equation 5 with $\theta = 0.50$, diffusion MGC is mostly likely in choosing $t^* = 2$ as the optimal time-step, and the testing power is almost equivalent to the best power among all $t \in \{0, 1, 2, \dots, 10\}$. The same phenomena hold for diffusion dCorr and diffusion HHG, and Figure 8b illustrates another RDPG simulation example by Equation 7. Indeed, the smoothing optimal technique for t^* has always achieved satisfactory performance throughout the experiments, which does not rely on cross validation or multiple testing.

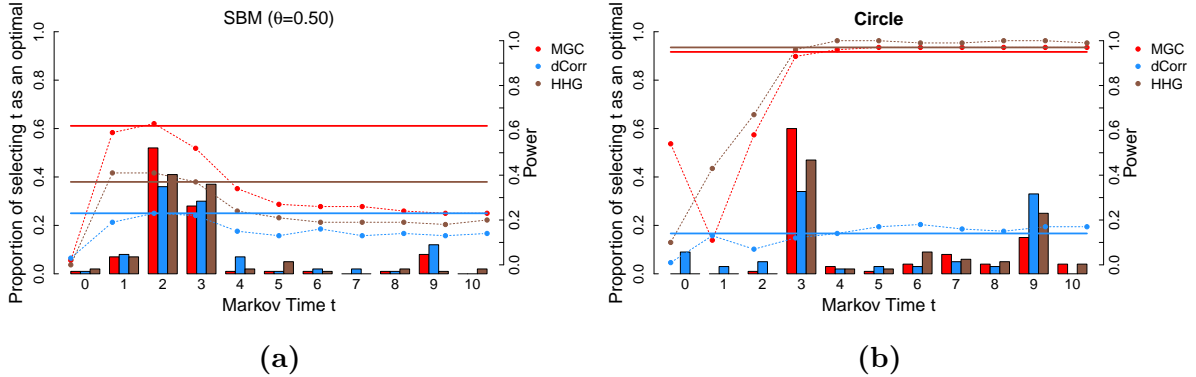


Figure 8: Testing power comparison between DMGC and MGC on each diffusion map. Using $nr = 100$ replicates, the solid red line plots the power of $MGC^*(\{U_n^t\}, X_n)$; the dash line plots the power of $MGC(U_n^t, X_n)$ for $t \in \{0, 1, 2, \dots, 10\}$; the bar plot shows the proportion that diffusion MGC selects each $t \in \{0, 1, 2, \dots, 10\}$ as the optimal t^* . Diffusion HHG and diffusion dCorr are also added by different colors. For each method, the diffusion statistic is able to achieve an excellent power that is almost equivalent to the best possible power among all t .

4.6 Real Data Experiment with Contamination

To demonstrate the application of the proposed method in real data, we test independence upon the brain network, where each node indicates voxel in the brain and edges represent brain fibers connecting each region (Kiar et al., 016a). Along with the information of the functional connectivity between the voxels, the data also provide the physical locations of each voxel in the brain represented by 3-dimensional voxel-wise coordinates. The brain network has been constructed by combining dMRI and sMRI data using the `ndmg` tool (Kiar et al., 2016).

The whole brain network data itself contain millions of nodes, so it is highly time-consuming to use all data for testing. As it is a common practice to sub-sample a small portion of big data for testing (under the assumption that significant relationship within the sub-sample is representative of the full data), we randomly selected one connected compo-

ment having 95 nodes and 337 edges to test dependency between the functional connectivity versus each voxel’s physical location. Moreover, we consider data contamination by edge flipping of the adjacency matrix: at contamination rate $c\%$, we randomly select $c\%$ of ones in the adjacency matrix and make them zeros, then randomly select $c\%$ of non-diagonal zeros and make them ones. Therefore, $c = 0$ equals the original data, while $c = 100$ flips all edges and it is merely a transformation of the original graph. Figure 9 shows empirical

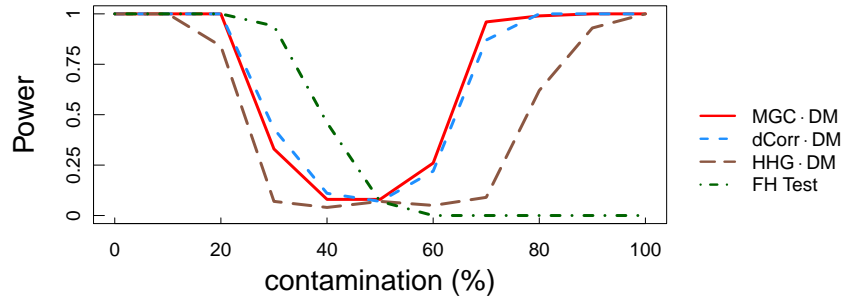


Figure 9: Powers are obtained through $nr = 100$ random contaminations for each of contamination level $c\% \in \{10\%, 20\%, \dots, 90\%\}$. As the level of contamination increases, it is less likely to reject the independence hypothesis with the FH Test than with our proposed approach.

power against the level of contamination $c\%$. Among the diffusion maps-based tests, MGC and dCorr maintain the overall best performance under the assumption of true dependence; while FH test is able to yield better power for $c \in [30, 50]$, the power quickly diminishes for $c > 50$. Note that as there is only one p-value to report at $c = 0$ and $c = 100$, the power is determined by whether each of p-value less than $\alpha = 0.05$ or not. At other choices of c , we randomly contaminate the data for $nr = 100$ replicates and report the proportion of rejecting the null at $\alpha = 0.05$.

5 Conclusion

In this study, we propose a new method for testing dependency on network data via diffusion maps as generalized graph Laplacian embeddings. The utilization of graph embeddings not only warrants the integration with various types of distance-based correlations, but also makes the testing method robust against parameter mis-specification that often plagues existing approaches. Applying multiscale generalized correlation allows the test to detect a wide range of nonlinear, high-dimensional, and noisy dependencies. Furthermore, employing multiple embeddings and computing a smoothed maximum test statistic overcome issues like multiple testing and cross validation, and largely mitigate the information loss problem that may occur to any single embedding choice. Therefore, the proposed DMGC approach is able to incorporate embedding theory, distance correlation, and post-selection inference together into a valid, consistent, and interpretable test procedure, which in turn achieves significant power improvement over existing methods.

There are several follow-ups that would further advance the work. First, it would be desirable to theoretically prove the robustness of the diffusion maps against q , and further investigate the relationship between q and t . Second, it will be straightforward to explore the applications to two-sample testing on graphs, or graphs with only partial correspondence. Third, the framework proposed in this paper also defines a good dependence measure on networks, thereby enabling many popular statistical techniques to be utilized on networks, like feature screening via distance correlation (Li et al., 2012).

References

- Chen, L., Shen, C., Vogelstein, J. T., and Priebe, C. E. (2016). Robust vertex classification. *IEEE Transactions on Pattern Analysis and Machine Intelligence*, 38(3):578–590.
- Coifman, R. R. and Lafon, S. (2006). Diffusion maps. *Applied and computational harmonic analysis*, 21(1):5–30.
- Coifman, R. R., Lafon, S., Lee, A. B., Maggioni, M., Nadler, B., Warner, F., and Zucker, S. W. (2005). Geometric diffusions as a tool for harmonic analysis and structure definition of data: Diffusion maps. *Proceedings of the National Academy of Sciences of the United States of America*, 102(21):7426–7431.
- Diaconis, P. and Freedman, D. (1980). Finite exchangeable sequences. *The Annals of Probability*, pages 745–764.
- Fosdick, B. K. and Hoff, P. D. (2015). Testing and modeling dependencies between a network and nodal attributes. *Journal of the American Statistical Association*, 110(511):1047–1056.
- Gretton, A. and Györfi, L. (2010). Consistent nonparametric tests of independence. *Journal of Machine Learning Research*, 11:1391–1423.
- Heller, R., Heller, Y., and Gorfine, M. (2013). A consistent multivariate test of association based on ranks of distances. *Biometrika*, 100(2):503–510.
- Heller, R., Heller, Y., Kaufman, S., Brill, B., and Gorfine, M. (2016). Consistent distribution-free k -sample and independence tests for univariate random variables. *Journal of Machine Learning Research*, 17(29):1–54.

- Howard, M., Cox Pahnke, E., Boeker, W., et al. (2016). Understanding network formation in strategy research: Exponential random graph models. *Strategic Management Journal*, 37(1):22–44.
- Inoue, H. and Taylor, R. (2006). Laws of large numbers for exchangeable random sets in kuratowski-mosco sense. *Stochastic Analysis and Applications*, 24(2):263–275.
- Karrer, B. and Newman, M. E. (2011). Stochastic blockmodels and community structure in networks. *Physical Review E*, 83(1):016107.
- Kiar, G., Gorgolewski, K. J., Kleissas, D., Roncal, W. G., Litt, B., Wandell, B., Poldrack, R. A., Wiener, M., Vogelstein, R. J., Burns, R., et al. (2016). Science in the cloud (sic): A use case in mri connectomics. *arXiv preprint arXiv:1610.08484*.
- Kiar, G., Roncal, W. G., Mhembe, D., Bridgeford, E., Burns, R., and Vogelstein, J. (2016a). ndmg: Neurodatas mri graphs pipeline.
- Koroljuk, V. S. and Borovskich, Y. V. (1994). *Theory of U-statistics*. Springer Science+Business Media Dordrecht.
- Lafon, S. and Lee, A. B. (2006). Diffusion maps and coarse-graining: A unified framework for dimensionality reduction, graph partitioning, and data set parameterization. *IEEE transactions on pattern analysis and machine intelligence*, 28(9):1393–1403.
- Li, R., Zhong, W., and Zhu, L. (2012). Feature screening via distance correlation learning. *Journal of American Statistical Association*, 107:1129–1139.
- Mantel, N. (1967). The detection of disease clustering and a generalized regression approach. *Cancer Research*, 27(2):209–220.

- Orbanz, P. and Roy, D. M. (2015). Bayesian models of graphs, arrays and other exchangeable random structures. *IEEE transactions on pattern analysis and machine intelligence*, 37(2):437–461.
- Pearson, K. (1895). Notes on regression and inheritance in the case of two parents. *Proceedings of the Royal Society of London*, 58:240–242.
- Peel, L., Larremore, D. B., and Clauset, A. (2017). The ground truth about metadata and community detection in networks. *Science Advances*.
- Rizzo, M. and Székely, G. (2016). Energy distance. *Wiley Interdisciplinary Reviews: Computational Statistics*, 8(1):27–38.
- Rohe, K., Chatterjee, S., and Yu, B. (2011). Spectral clustering and the high-dimensional stochastic blockmodel. *The Annals of Statistics*, pages 1878–1915.
- Shen, C., Priebe, C. E., and Vogelstein, J. T. (2017a). From distance correlation to multi-scale generalized correlation. *arXiv preprint arXiv:1710.09768*.
- Shen, C., Priebe, C. E., Wang, Q., Maggioni, M., and Vogelstein, J. T. (2017b). Discovering relationships and their structures across disparate data modalities. *arXiv preprint arXiv:1609.05148*.
- Sussman, D., Tang, M., Fishkind, D., and Priebe, C. (2012). A consistent adjacency spectral embedding for stochastic blockmodel graphs. *Journal of the American Statistical Association*, 107(499):1119–1128.
- Sussman, D. L., Tang, M., and Priebe, C. E. (2014). Consistent latent position estimation and vertex classification for random dot product graphs. *IEEE transactions on pattern analysis and machine intelligence*, 36(1):48–57.

- Székely, G. and Rizzo, M. (2013a). The distance correlation t-test of independence in high dimension. *Journal of Multivariate Analysis*, 117:193–213.
- Székely, G. and Rizzo, M. (2014). Partial distance correlation with methods for dissimilarities. *Annals of Statistics*, 42(6):2382–2412.
- Székely, G. J. and Rizzo, M. L. (2013b). The distance correlation t-test of independence in high dimension. *Journal of Multivariate Analysis*, 117:193–213.
- Székely, G. J., Rizzo, M. L., Bakirov, N. K., et al. (2007). Measuring and testing dependence by correlation of distances. *The Annals of Statistics*, 35(6):2769–2794.
- Tang, M., Athreya, A., Sussman, D. L., Lyzinski, V., Park, Y., and Priebe, C. E. (2017a). A semiparametric two-sample hypothesis testing for random dot product graphs. *Journal of Computational and Graphical Statistics*, 26(2):344–354.
- Tang, M., Athreya, A., Sussman, D. L., Lyzinski, V., and Priebe, C. E. (2017b). A nonparametric two-sample hypothesis testing problem for random dot product graphs. *Bernoulli*, 23(3):1599–1630.
- Wasserman, S. and Pattison, P. (1996). Logit models and logistic regressions for social networks: I. an introduction to markov graphs andp. *Psychometrika*, 61(3):401–425.
- Zhu, M. and Ghodsi, A. (2006). Automatic dimensionality selection from the scree plot via the use of profile likelihood. *Computational Statistics and Data Analysis*, 51:918–930.

Acknowledgment

This work was partially supported by the National Science Foundation Division of

Mathematical Sciences award DMS-1712947, the National Security Science and Engineering Faculty Fellowship (NSSEFF), the Johns Hopkins University Human Language Technology Center of Excellence (JHU HLT COE), the Defense Advanced Research Projects Agency's (DARPA) SIMPLEX program through SPAWAR contract N66001-15-C-4041, the XDATA program of DARPA administered through Air Force Research Laboratory contract FA8750-12-2-0303. The authors thank Dr. Minh Tang, Dr. Daniel Sussman, and Dr. Carey Priebe for insightful suggestions, and the reviewers and editor for their valuable comments that greatly enhanced the paper.

APPENDIX

A Proofs

Unless mentioned otherwise, throughout the proof section we always omit the superscript t for the diffusion map at a fixed t , i.e., we use $U_n = \{u_i : i = 1, \dots, n\}$ instead of $U_n^t = \{u_i^t : i = 1, \dots, n\}$ because most results hold for any t .

Proof of Theorem 1. By the celebrated *de Finetti's Theorem* (Diaconis and Freedman, 1980; Orbanz and Roy, 2015), it suffices to prove that the diffusion map $U_n = \{u_i : i = 1, \dots, n\}$ is always exchangeable in distribution, i.e., for any n and all possible permutation σ , the permuted sequence $\{u_{\sigma(1)}, u_{\sigma(2)}, \dots, u_{\sigma(n)}\}$ always distributes the same as the original sequence $\{u_1, u_2, \dots, u_n\}$.

Transforming Equation 2 into matrix notation yields

$$U_n = \Lambda_n^t \Phi_n',$$

where U_n is the $q \times n$ matrix having u_i as its i^{th} column, $\Lambda_n = \text{diag}\{\lambda_1, \lambda_2, \dots, \lambda_q\}$ is the diagonal matrix having selected eigenvalues of L_n , $\Phi_n = [\phi_1, \phi_2, \dots, \phi_q]$ consists of the corresponding eigenvectors, \cdot^t denotes t^{th} power, and \cdot' is the matrix transpose. It suffices to show that U_n and $U_n \Pi_n$ are identically distributed for any permutation matrix Π_n of size n .

Given that the graph \mathbf{G} is an induced subgraph of an infinitely exchangeable graph, it holds that $A_n(\sigma(i), \sigma(j)) \stackrel{d}{=} A_n(i, j)$, which further holds for the symmetric graph Laplacian

L_n :

$$\begin{aligned}
L_n(\sigma(i), \sigma(j)) &= A_n(\sigma(i), \sigma(j)) / \left\{ \sum_j A_n(\sigma(i), \sigma(j)) \sum_i A_n(\sigma(i), \sigma(j)) \right\}^{1/2} \\
&\stackrel{d}{=} A_n(i, j) / \left\{ \sum_j A_n(i, j) \sum_i A_n(i, j) \right\}^{1/2} \\
&= L_n(i, j).
\end{aligned}$$

In matrix notation, $\Pi_n' L_n \Pi_n \stackrel{d}{=} L_n$ for any permutation matrix Π_n .

By eigen-decomposition, the first q eigenvalues and the corresponding eigenvector of $\Pi_n' L_n \Pi_n$ are Λ_n and $\Pi_n' \Phi_n$, so it follows that at any t

$$\begin{aligned}
\Phi_n &\stackrel{d}{=} \Pi_n' \Phi_n \\
\Leftrightarrow U_n &= \Lambda_n^t \Phi_n' \stackrel{d}{=} \Lambda_n^t \Phi_n' \Pi_n = U_n \Pi_n
\end{aligned}$$

Thus the diffusion maps are infinitely exchangeable. By the *de Finetti's Theorem*, there exists a latent variable \mathbf{u} such that $\{u_i : i = 1, \dots, n\}$ are *iid* asymptotically conditional on \mathbf{u} . □

Proof of Theorem 2. We first state three lemmas:

Lemma 1. Under the same assumptions of Theorem 2, for any finite time-step t , the latent variable \mathbf{u} of the diffusion map is of finite first moment.

Lemma 2 (Székely et al. (2007)). The distance covariance of $(U_n, X_n) = \{(u_i, x_i) : i = 1, \dots, n\}$ defined in Equation 3 is equivalent to

$$\mathrm{dCov}(U_n, X_n) = \int_{\mathbb{R}^{q+p}} |\hat{g}_{U_n, X_n}(t, s) - \hat{g}_{U_n}(t) \hat{g}_{X_n}(s)|^2 dw(t, s),$$

where $w(t, s) \in \mathbb{R}^q \times \mathbb{R}^p$ is a nonnegative weight function that equals $(c_q c_p |t|_q^{1+q} |s|_p^{1+p})^{-1}$, c_q is a nonnegative constant, \hat{g} is the empirical characteristic function of $\{(u_i, x_i) : i = 1, 2, \dots, n\}$ or the marginals, e.g., $\hat{g}_{U_n, X_n}(t, s) = \frac{1}{n} \sum_{i=1}^n \exp\{\mathbf{i} \langle t, u_i \rangle + \mathbf{i} \langle s, x_i \rangle\}$ with \mathbf{i} representing the imaginary unit.

Lemma 3 (Székely et al. (2007)). Assume $\{u_i : i = 1, 2, \dots, n\}$ are *iid* conditional on \mathbf{u} , and $\{x_i \stackrel{iid}{\sim} F_{\mathbf{x}}, i = 1, 2, \dots, n\}$, where \mathbf{u} and \mathbf{x} are both of finite first moment. It follows that

$$\mathrm{dCov}(U_n, X_n) \rightarrow \mathrm{dCov}(\mathbf{u}, \mathbf{x}) \text{ as } n \rightarrow \infty$$

where $\mathrm{dCov}(\mathbf{u}, \mathbf{x}) := \int_{\mathbb{R}^{q+p}} |g_{\mathbf{u}, \mathbf{x}}(t, s) - g_{\mathbf{u}}(t)g_{\mathbf{x}}(s)|^2 dw(t, s)$, and g is the characteristic function, i.e., $g_{\mathbf{u}, \mathbf{x}}(t, s) = E(\exp\{\mathbf{i} \langle t, \mathbf{u} \rangle + \mathbf{i} \langle s, \mathbf{x} \rangle\})$.

By Theorem 1, the diffusion maps U_n are asymptotically *iid* conditioned on \mathbf{u} , whose finite moment is guaranteed by Lemma 1. The nodal attributes X_n are *iid* as $F_{\mathbf{x}}$ of finite first moment as assumed in (C2). Therefore a direct application of Lemma 2 and Lemma 3 yields that

$$\mathrm{dCov}(U_n, X_n) \rightarrow \int_{\mathbb{R}^{q+p}} |g_{\mathbf{u}, \mathbf{x}}(t, s) - g_{\mathbf{u}}(t)g_{\mathbf{x}}(s)|^2 dw(t, s),$$

which equals 0 if and only if \mathbf{u} is independent of \mathbf{x} . As distance correlation is just a normalized version of distance covariance, it further leads to

$$\mathrm{dCorr}(U_n, X_n) \rightarrow c \geq 0, \tag{8}$$

for which the equality holds if and only if \mathbf{u} is independent of \mathbf{x} . By Shen et al. (2017a),

Equation 8 also holds for **MGC** when it holds for **dCorr**. \square

Proof of Lemma 1. To prove that \mathbf{u} is of finite first moment, it suffices to show that $\|u_i\|_2$ is always bounded for all $i \in [1, n]$.

By Equation 2, we have

$$\begin{aligned} \|u_i\|_2^2 &= \sum_{j=1}^q \lambda_j^{2t} \phi_j^2(i) \\ &\leq \sum_{j=1}^q \lambda_j^{2t} \\ &\leq q, \end{aligned}$$

where the second line follows by noting $\phi_j(i) \in [-1, 1]$ (the eigenvector ϕ_j is always of unit norm), and the third line follows by observing that $|\lambda_j| \leq \|L_n\|_\infty = 1$.

Therefore, all of u_i are bounded in ℓ_2 norm as $n \rightarrow \infty$, so the latent variable \mathbf{u} must be of finite first moment for any finite t . \square

Proof of Lemma 2. This lemma is a direct application of Theorem 1 in Székely et al. (2007), which holds without any assumption on $(U_n, X_n) = \{(u_i, x_i) : i = 1, 2, \dots, n\}$, e.g., it holds without assuming exchange-ability, nor identically distributed, nor finite first moment. \square

Proof of Lemma 3. This lemma is equivalent to Theorem 2 in Székely et al. (2007), except the *iid* assumption is replaced by exchangeable assumption, i.e., the original set-up assumes $(U_n, X_n) = \{(u_i, x_i) : i = 1, 2, \dots, n\}$ is independently identically distributed as (\mathbf{u}, \mathbf{x}) with finite first moment; whereas the diffusion map $\{u_i : i = 1, 2, \dots, n\}$ is asymptotically conditional *iid* with finite first moment.

All major steps in proving Theorem 2 of Székely et al. (2007) are essentially the same for either *iid* random variables or infinitely exchangeable random variables (Inoue and Taylor, 2006). In particular, under the finite moment assumption, we still have the large number for V-statistics (Koroljuk and Borovskich, 1994), i.e.,

$$\int_{D(\delta)} |\hat{g}_{\mathbf{u},\mathbf{x}}(t, s) - \hat{g}_{\mathbf{u}}(t)\hat{g}_{\mathbf{x}}(s)|^2 dw \xrightarrow{n \rightarrow \infty} \int_{D(\delta)} |g_{\mathbf{u},\mathbf{x}}(t, s) - g_{\mathbf{u}}(t)g_{\mathbf{x}}(s)|^2 dw,$$

where $D(\delta) = \{(t, s) : \delta \leq |t|_q \leq 1/\delta, \delta \leq |s|_p \leq 1/\delta\}$. □

Proof of Theorem 3. From Theorem 2, it holds that

$$\mathbf{MGC}(U_n^t, X_n) \rightarrow c \geq 0 \tag{9}$$

for each t , with equality if and only if \mathbf{u}^t is independent of \mathbf{x} . The DMGC algorithm enforces that

$$\max\{\mathbf{MGC}(U_n^t, X_n), t = 0, 1, \dots, 10\} \geq \mathbf{MGC}^*({U_n^t}, X_n) \geq \mathbf{MGC}(U_n^{t=3}, X_n),$$

thus Equation 9 also holds when $\mathbf{MGC}(U_n^t, X_n)$ is replaced by $\mathbf{MGC}^*({U_n^t}, X_n)$.

Under the permutation test, MGC combined with diffusion maps is valid because: when each column of U_n^t and X_n are independent, so are U_n^t versus any permuted copy $X_n\Pi_n$. Then the p-value of DMGC is always uniformly distributed in $[0, 1]$, and the type 1 error level is correctly controlled.

DMGC is consistent because $\mathbf{MGC}^*({U_n^t}, X_n)$ converges to a positive number under dependence, and 0 otherwise. As the percentage of partial derangement of fixed sizes converges to 1, $X_n\Pi_n$ is asymptotically almost surely independent of U_n^t (a more thorough analysis

on partial derangement on permutation is provided in Shen et al. (2017a)), i.e.,

$$Prob[\text{MGC}^*(\{U_n^t\}, X_n) \geq \text{MGC}^*(\{U_n^t\}, X_n \Pi_n)] \rightarrow 0$$

for any permutation matrix Π_n of size n as $n \rightarrow \infty$. Thus the p-value under dependence and permutation test is asymptotically 0, and consistency for testing \mathbf{u}^t versus \mathbf{x} holds at any type 1 error level.

Moreover, when the transformation from A_n to U_n^t is injective, we have

$$\begin{aligned} & \mathbf{a} \text{ is independent of } \mathbf{x} \\ \Leftrightarrow & A_n \text{ is independent of } X_n \text{ in distribution} \\ \Leftrightarrow & U_n^t \text{ is independent of } X_n \text{ in distribution} \\ \Leftrightarrow & \text{MGC}(U_n^t, X_n) \text{ is asymptotically } 0, \end{aligned}$$

where the second line follows because each column of A_n is assumed identically distributed as $F_{\mathbf{a}}$ in Equation 1, the third line follows from injective transformation, and the last line follows from Theorem 1 and Theorem 2. Once the last line is established, DMGC is consistent between A_n and X_n .

Note that without the injective condition on A_n and U_n^t , the reverse direction of the third line may not always hold, i.e., when the diffusion maps are independent from the nodal attributes, the adjacency matrix may be still dependent with the nodal attributes. In that case, DMGC is still valid but the dependency may not be detected by DMGC. \square

Proof of Corollary 1. (1) When the nodal attribute is replaced by a second graph with the same node set as the first graph, we simply compute the diffusion map of the second graph by the same procedure as for the first graph.

(2) Changing the test statistic only affects Theorem 2. Both **dCorr** and **MGC** satisfy Theorem 2 directly, while **HHG** is also a statistic that is 0 if and only if independence (Heller et al., 2013).

(3) When A_n is symmetric and binary, the transformation from A_n to L_n is injective, i.e., two different A_n always produce two different L_n . Then for each unique L_n , the eigen-decomposition is always unique such that L_n to $U_n^{t=1}$ is injective, provided that the dimension choice is made correct at q . \square

Proof of Corollary 2. From Proposition 1 and 2, U_n^1 is asymptotically equivalent to the latent positions W_n up-to a bijection. Moreover, under RDPG, if two different adjacency matrices yield the same U_n^1 , they must asymptotically equal the same latent positions and asymptotically the same adjacency matrix (i.e., the difference in Frobenius norm converges to 0). Therefore injective holds asymptotically, and Theorem 3 applies. \square

B Random Dot Product Graph Simulations

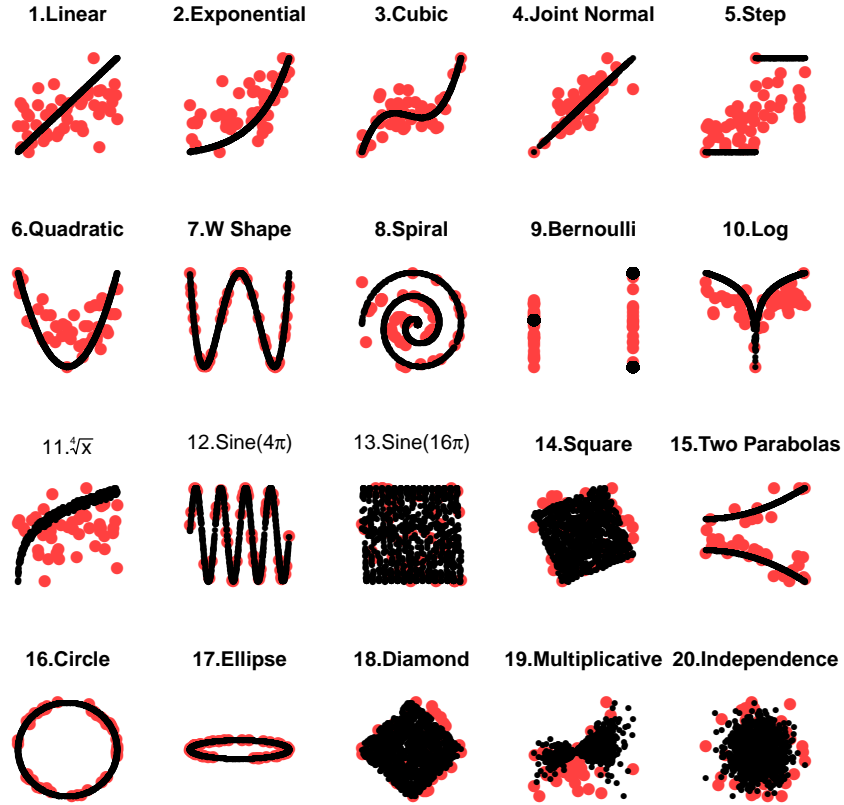


Figure E1: Illustrations of randomly generated $n = 50$ points of $\{(w_i, x_i) : i = 1, 2, \dots, 50\}$ (red dots) along with their population version without noise (black dots).

For the 20 simulations under RDPG, we describe the generating distribution $(\tilde{w}_i, \tilde{x}_i) \stackrel{iid}{\sim} F_{\tilde{w}, \tilde{x}}$ under each scenario. Visualization for the sample observations of (W_n, X_n) at $n = 50$ is shown in Figure E1. Notation-wise, $\mathcal{N}(\mu, \sigma)$ denotes the normal distribution with mean μ and standard deviation σ , $\mathcal{U}[a, b]$ denotes the uniform distribution from a to b , $\mathcal{B}(p)$

denotes the Bernoulli distribution with probability p , and ϵ_i denotes white noise.

1. Linear

$$\tilde{w}_i \sim \mathcal{U}[0, 1], \quad \epsilon_i \sim \mathcal{N}(0, 0.5),$$

$$\tilde{x}_i = \tilde{w}_i + \epsilon_i.$$

2. Exponential

$$\tilde{w}_i \sim \mathcal{U}[0, 3], \quad \epsilon_i \sim \mathcal{N}(0, 5),$$

$$\tilde{x}_i = \exp(\tilde{w}_i) + \epsilon_i.$$

3. Cubic

$$\tilde{w}_i \sim \mathcal{U}[0, 1], \quad \epsilon_i \sim \mathcal{N}(0, 0.5),$$

$$\tilde{x}_i = 20(\tilde{w}_i - 0.5)^3 + 2(\tilde{w}_i - 0.5)^2 - (\tilde{w}_i - 0.5) + \epsilon_i.$$

4. Joint Normal

$$(\tilde{w}_i, \tilde{x}_i) \sim \mathcal{N} \left(\begin{bmatrix} 0 \\ 0 \end{bmatrix}, \begin{bmatrix} 0.7 & 0.5 \\ 0.5 & 0.7 \end{bmatrix} \right).$$

5. Step Function

$$\tilde{w}_i \sim \mathcal{U}[-1, 1], \quad \epsilon_i \sim \mathcal{N}(0, 0.5),$$

$$\tilde{x}_i = \mathbf{I}(\tilde{w}_i > 0) + \epsilon_i.$$

6. Quadratic

$$\begin{aligned}\tilde{w}_i &\sim \mathcal{U}[-1, 1], \quad \epsilon_i \sim \mathcal{N}(0, 0.3), \\ \tilde{x}_i &= \tilde{w}_i^2 + \epsilon_i.\end{aligned}$$

7. W Shape

$$\begin{aligned}\tilde{w}_i &\sim \mathcal{U}[-1, 1] \\ \tilde{x}_i &= 4(\tilde{w}_i^2 - 0.5)^2\end{aligned}$$

8. Spiral

$$\begin{aligned}z_i &\sim \mathcal{U}[0, 5], \quad \epsilon_i \sim \mathcal{N}(0, 0.1), \\ \tilde{w}_i &= z_i \cos(z_i \pi), \\ \tilde{x}_i &= z_i \sin(z_i \pi) + \epsilon_i.\end{aligned}$$

9. Bernoulli

$$\begin{aligned}\tilde{w}_i &\sim \mathcal{B}(0.5), \quad \epsilon_i \sim \mathcal{N}(0, 1), \\ \tilde{x}_i &= (2\mathcal{B}(0.5) - 1)\tilde{w}_i + \epsilon_i.\end{aligned}$$

10. Logarithm

$$\begin{aligned}\tilde{w}_i &\sim \mathcal{U}[-1, 1], \quad \epsilon_i \sim \mathcal{N}(0, 5), \\ \tilde{x}_i &= 5 \log_2(|\tilde{w}_i|) + \epsilon_i.\end{aligned}$$

11. Fourth Root

$$\begin{aligned}\tilde{w}_i &\sim \mathcal{U}[0, 1], \quad \epsilon_i \sim \mathcal{N}(0, 0.5), \\ \tilde{x}_i &= (|\tilde{w}_i + \epsilon_i|)^{1/4}.\end{aligned}$$

12. Sine Period 4π

$$\begin{aligned}\tilde{w}_i &\sim \mathcal{U}[-1, 1], \quad \epsilon_i \sim \mathcal{N}(0, 0.01), \\ \tilde{x}_i &= \sin(4\tilde{w}_i\pi) + \epsilon_i.\end{aligned}$$

13. Sine Period 16π

$$\begin{aligned}\tilde{w}_i &\sim \mathcal{U}[-1, 1], \quad \epsilon_i \sim \mathcal{N}(0, 0.01), \\ \tilde{x}_i &= \sin(16\tilde{w}_i\pi) + \epsilon_i.\end{aligned}$$

14. Square

$$\begin{aligned}u_{i1} &\sim \mathcal{U}[-1, 1], \quad u_{i2} \sim \mathcal{U}[-1, 1], \\ \tilde{w}_i &= u_{i1} \cos(-\pi/8) + u_{i2} \sin(-\pi/8), \\ \tilde{x}_i &= -u_{i1} \sin(-\pi/8) + u_{i2} \cos(-\pi/8).\end{aligned}$$

15. Two Parabolas

$$\tilde{z}_i \sim \mathcal{B}(0.3), \quad \epsilon_i \sim \mathcal{N}(0.5, 0.3),$$

$$\tilde{w}_i \sim \mathcal{U}[0, 1],$$

$$\tilde{x}_i = (\tilde{w}_i^2 + \epsilon_i)(\tilde{z}_i - 0.5).$$

16. Circle

$$u_i \sim \mathcal{U}[-1, 1], \quad \epsilon_i \sim \mathcal{N}(0, 0.05),$$

$$\tilde{w}_i = \cos(u_i\pi),$$

$$\tilde{x}_i = \sin(u_i\pi) + \epsilon_i.$$

17. Ellipse

$$u_i \sim \mathcal{U}[-1, 1],$$

$$\tilde{w}_i = 5 \cos(u_i\pi),$$

$$\tilde{x}_i = \sin(u_i\pi).$$

18. Diamond

$$u_{i1} \sim \mathcal{U}[-1, 1], \quad u_{i2} \sim \mathcal{U}[-1, 1],$$

$$\tilde{w}_i = u_{i1} \cos(-\pi/4) + u_{i2} \sin(-\pi/4),$$

$$\tilde{x}_i = -u_{i1} \sin(-\pi/4) + u_{i2} \cos(-\pi/4).$$

19. Multiplicative Noise

$$\begin{aligned}\tilde{w}_i &\sim \mathcal{N}(0.5, 1), \quad \epsilon_i \sim \mathcal{N}(0.5, 1), \\ \tilde{x}_i &= \tilde{w}_i \cdot \epsilon_i\end{aligned}$$

20. Independence

$$\begin{aligned}\tilde{w}_i &\sim \mathcal{N}(0, 1) \\ \tilde{x}_i &\sim \mathcal{U}(0, 1)\end{aligned}$$

C Two-graph Testing under the Random Dot Product Graph

Here we apply the network dependence test approach to testing independence between two graphs from RDPG model; this is essentially equivalent to testing independence between each of diffusion map embedding as mentioned in Corollary 1. As we are given two graphs, it becomes more challenging to choose the “optimal” embedding in terms of Markov iteration time as we have an option of $\mathbb{N} \times \mathbb{N}$ space to choose distinct t for each graph. For simplicity we assume that the optimal t^* is identical between the two graphs so that we only need to search t^* which maximizes the dependency among the pairs of diffusion maps both evaluated at $t \in \{0, 1, 2, \dots, 10\}$. This restriction can be released at the cost of computational burden.

Assume two graphs \mathbf{G}_1 and \mathbf{G}_2 having an adjacency matrix of $A_n^{(1)}$ and $A_n^{(2)}$ respectively

are generated via a latent variable $Z_n = \{z_i \in \mathbb{R}^5 : i = 1, 2, \dots, n\}$ as follows:

$$\begin{aligned}
 z_{ik} &\stackrel{iid}{\sim} \text{Unif}(0, 1), \quad i = 1, 2, \dots, n; \quad k = 1, 2, \dots, 5 \\
 w_i &:= (1 - z_{i1})^2, \quad i = 1, 2, \dots, n \\
 \mathbf{A}_n^{(1)}(i, j) | z_i, z_j &\sim \text{Bernoulli}(\langle z_i/5, z_j/5 \rangle), \quad \forall i < j; \quad i, j = 1, 2, \dots, n \\
 \mathbf{A}_n^{(2)}(i, j) | w_i, w_j &\sim \text{Bernoulli}(\langle w_i, w_j \rangle), \quad \forall i < j; \quad i, j = 1, 2, \dots, n.
 \end{aligned} \tag{10}$$

Namely, each graph is generated by a random dot product graph, and the underlying dependency is reflected via the quadratic function of one-dimensional latent variable; this implies both multi-dimensional and nonlinear relationship where MGC is preferred to other benchmarks in testing network dependency in nodal attributes. Figure E2 shows the testing

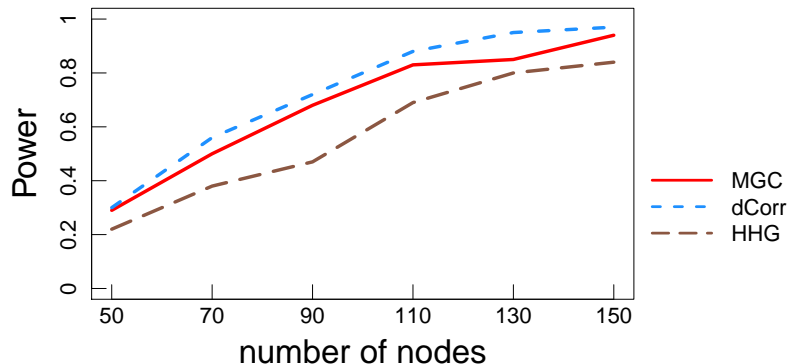


Figure E2: The power curve with respect to increasing number of nodes for the a paired graph-test simulation (Equation 10). MGC and dCorr achieve a perfect power faster than HHG, and FH test is not applicable in this case.

power of MGC, dCorr, and HHG against the number of nodes n , all based on the diffusion maps, and it demonstrates that the proposed approach is able to achieve higher testing power under relatively small number of nodes. Note that if noise is included in the setup, or the nonlinear relationship is more complex than quadratic, the proposed approach

still enjoys the same advantage, i.e., the testing power converges to 1 faster than all other methods (similar to the simulations in [Shen et al. \(2017b\)](#)), though the actual number of nodes to achieve perfect power will likely increase under noisy and complex dependency.